Volume 16, Issue 1, 162506 (1-10)

International Journal of Nano Dimension (IJND)

https://dx.doi.org/10.57647/j.ijnd.2025.1601.06

Bio synthesis and characterization of Ni doped CuO nanocomposite using *Centratherum punctatum* leaf extract

Subramanian Subha[1]*, Muthukurumban Nagarajan[1], Selvaraj Saseetha[1], Subbiah Chelladurai Vella Durai[2]

[1]*Department of Physics, V.O.Chidambaram College, Thoothukudi, Tamilnadu, India.*
[2]*PG and Research Department of Physics, Sri Paramakalyani College, Alwarkurichi, Tenkasi, Tamilnadu, India.*

*Corresponding author: ssadhithya@gmail.com

Original Research

Received:
19 August 2024
Revised:
15 September 2024
Accepted:
26 September 2024
Published online:
10 January 2025

Abstract:

Pristine and Nickel doped Copper Oxide (CuO) nanocomposite were synthesized using Centratherum Punctatum leaf extract. The structural characterization is performed employing XRD, SEM, and EDAX. Pure Copper Oxide nanoparticles (CuO Nps) exhibit leaf-like morphology, but Nickel-doped Copper Oxide nanocomposites exhibit a mixture of rod, spherical and hexagonal morphology. Owing to the XRD data, the resulting particles for NiO NPs, CuO NPs, and Ni-doped CuO nanocomposite comprised crystallite sizes of 35 nm, 41 nm, and 37 nm, respectively. The optical properties and functional group of the materials are analyzed utilizing UV-Vis and FTIR. The rise in the measured optical band gap values was seen by the blue shift noted in the UV-vis study subsequent to nickel doping. The existence of different functional groups in samples is verified by FT-IR characterization. The electrochemical analysis is studied by cyclic voltammetry. It exhibits an elevated specific capacitance value of 314 F/g for Ni doped copper oxide nanocomposite. The antibacterial activity studies reveal that the Ni-doped nanocomposite is active against gram-negative bacteria over and above the gram-positive bacterial species.

Keywords: Antibacterial; Centratherum Punctatum leaves; Cyclic voltammetry; Electrochemical; Morphology; Nanocomposites

1. Introduction

Recent years have witnessed a rise in interest in nanomaterials owing to their distinct chemical and physical characteristics. The experimental settings used to prepare these materials significantly affect the product's particle size [1]. The manufacture of metal oxide nanoparticles has garnered substantial attention in recent decades because of their wide range of applications, including optoelectronics, nanodevices, nanoelectronics, nanosensors, and catalysis. Multiple investigations point out that nanoparticles have distinct toxicity profiles compared to bigger fragments because of their small size and strong reactivity [2]. Metal oxide nanoparticles are fascinating to the scientific and industrial sectors because of their distinctive optical, magnetic, electrical, and chemical features caused by their high surface area - to - volume ratio [3]. Within these compounds is copper oxide (CuO), a P - type metal oxide with a 1.4 eV band gap and a monoclinic structure that might find use in solar cells, sensors, optoelectronic devices, catalysts, and lithium ion batteries. In contrast to the semiconductor material as a single compound, the addition of appropriate impurities to the metal oxide matrix results in improved physico-chemical properties that may be used in new device applications [4]. Early research has reported on metal oxide doped with several transition metal ions, including Mn, Fe, and Sn, in the copper oxide lattice structure [5, 6]. Ni is regarded as the ideal transitional metal dopant among them all for applications requiring high energy and power density. NiO nanoparticles are p-type semiconductors with a broad band gap of 3.6 to 4.0 eV [7]. Because of their superior physico-chemical characteristics, they are a promising option for advanced material applications, including gas sensors and electronic devices [8], active anode material for Li-ion batteries, electrode material for super capacitors [9], and catalysts for electrochemical reactions [10]. Many unique techniques, including sol-gel, chemical precipita-

tion, ball milling, microwave-assisted process, hydrothermal, combustion, and mechanical alloying, produce metal oxide nanoparticles [11]. Particularly, the biological mode is preferred over the available physical, chemical, and biological approaches for the fabrication of metal nanoparticles (NPs) due to its advantages, which include reduced energy requirements, biocompatibility, sustainability, non-toxic reagents, enhanced stability, ease of processing, and the removal of unnecessary processing during synthesis. In contrast, physicochemical methods are costly and may result in toxic by products. The organic biomolecules have two roles in the biological creation of metal nanoparticles (NPs): they stabilize and reduce the NPs. It has been demonstrated that the biomolecules such as flavones, phenolics, and glycosides surround the nanoparticles and create a stable colloidal system in addition to reducing the metal ions and converting them to their nanoforms [12–14]. Plants such as Calotropis procera leaf extract , Abutilon indicum leaf extract , aloe vera leaf extract , karaya gum , Cassia alata flower extract, Caesalpinia bonducella seed extract, Punica granatum peel extract, Ixiro coccinea plant leaves, Gum Acacia, Eupatorium adenophorum, etc. are reported to be utilized during the green synthesis of CuO NPs in the literature [15–18].

Hence, the present work focuses on synthesizing CuO, NiO, and Ni doped CuO nanocomposite using *Centratherum punctutam* leaf extract and studying the various characteristics. It is also termed as the 'Queen of all Herbs' and is closely related to *Centratheruman thelmethicum* plant, known for high medicinal value. *Centratherum punctatum* used in traditional drugs and belongs to the family of *Asteraceae*. It is an everlasting bushy plant 45-60 cm tall with a well-stemmed and purple colour flower head [19, 20]. It is used to treat a number of illnesses, including pain, fever, digestive problems, inflammation, and cancer [21] . The Nùng and Tày ethnic communities in Thailand utilize the plant to treat flu-like illnesses and jaundice. They also use the plant's decoction to bathe women after giving birth [22]. The herb has qualities that are anti-inflammatory [23], anti-oxidant, anti-proliferative, anti-fungal and antibacterial [24]. Many beneficial phytochemicals have been found in Centratherum. punctatum, including sesquiterpene lactones, flavones, phenolics, and glycosides. These include anti-cancerous substances like eugenol, spathulenol, sqalene, viridiflorol, and eicosane, among others. This plant has also been investigated for its cytotoxic, anti plasmodial, HIV-1 reverse transcriptase inhibitory, and molluscisidal properties [25]. It offers anti-aging, skin-whitening, and hair-care benefits in addition to being used as an analgesic and remedy for tiger and snake bites. The plants floral extracts exhibit protease activity, which contributes to the plant's ability to heal wounds [26]. CuO, NiO, and Ni-doped CuO nanocomposite production is mostly carried out by the phytochemical flavonoids, which also serve as reducing and stabilizing agents.

To the best of our knowledge, there is no study available on the environmentally friendly synthesis of CuO NPs, NiO NPs, and Ni-doped CuO nanocomposite utilizing *Centratherum punctatum* leaf extract. In this work, the green synthesis of CuO, NiO NPs, and Ni-doped CuO nanocomposite is investigated, along with their characterization and antibacterial activity. Leaf extract can be used to alter the size and form of the particles while also preventing nanoparticle aggregation.

2. Materials and Methods

2.1 Chemicals

Copper Chloride, Nickel Chloride, Sodium Hydroxide and *Centratherum punctutam* leaves were used. Sodium Hydroxide is used for pH adjustment.

2.2 Extract preparation

Fresh leaves of *Centratherum punctutam* were collected and thoroughly washed with distilled water. After drying, the leaves were cut into small pieces. Ten grams of the cleaned *Centratherum punctutam* were soaked in 100 mL of deionized water, and heated on a hot plate at 80 ^{O}C for one hour. The plant extract was then allowed to cool and filtered (using Whatmann filter paper), obtain a pure aqueous extract. The pH of the extract was measured at 5.5. This extract can be stored in the refrigerator for up to three days.

2.3 Green syntheseis of NiO/CuO Nps and Ni-doped CuO nanocomposite

To synthesize NiO Nps (0.1 M), a 100 mL solution of Nickel Chloride ($NiCl_2.6H_2O$) was prepared. From this, 40 mL was combined with a leaf extract solution that had its pH adjusted. The mixture was stirred for one hour, during which the color shifted from light green to dark green, and a brown precipitate formed. For CuO Nps (0.1 M), a similar procedure was followed: 100 mL of Copper Chloride ($CuCl_2.2H_2O$) solution was prepared and 40 mL of it was mixed with the leaf extract. After one hour of stirring, the color changed from bluish green to dark green, and a brown precipitate appeared. The Ni-doped CuO nanocomposite was synthesized with modifications based on the method of Soruma Gudina Firisa. Separate 50 mL solutions of copper chloride and 10 mL solutions of nickel chloride were prepared at 0.1 M concentration. To synthesize CuO Nps, 20 mL of the leaf extract was added to the copper chloride solution and stirred for 30 minutes. The nickel chloride solution was then added drop by drop, and the mixture was stirred continuously for two hours at room temperature. The resulting precipitate was washed multiple times with deionized water to remove impurities, filtered using Whatman No. 1 filter paper, and dried at 100 ^{O}C. The product was then calcined for one hour at 500 ^{O}C. Finally, the black-colored NiO and CuO Nps were collected and stored for further characterization.

3. Results and discussions

3.1 XRD analysis

Figure 1. shows the XRD pattern of pure NiO, CuO and Ni doped CuO. The diffraction peaks of NiO Nps observed at 36.95 ^{O}, 43.00 ^{O}, 62.78 ^{O}, 75.12 ^{O} and 79.37 ^{O} belong to (111), (200), (220), (311) and (222) hkl values. It exhibits

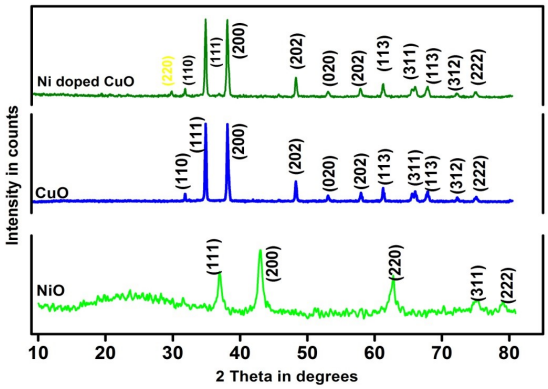

Figure 1. XRD of pure NiO, pure CuO, and Ni doped CuO nanocomposite.

a face centred cubic system (FCC) belonging to the space group of (Fm3 m) [27, 28]. The values are well matched with JCPDS card No 04-835. The average particle size of NiO is around 35 nm calculated using the Scherer formula. In CuO Nps, the peaks obtained at 32.49 ^{O}, 35.48 ^{O}, 38.86 ^{O},46.26 ^{O}, 48.78 ^{O}, 53.55 ^{O}, 58.19 ^{O}, 61.53 ^{O}, 66.84 ^{O}, 72.06 ^{O}, and 75.39 ^{O} corresponding to reflection from (110), (111), (200), (202), (020), (202), (113), (311), (113), (312), and (222) are well matched with JCPDS card no. 48-1548. It shows that the Nps are monoclinic crystalline structures with an average particle size of 41 nm. In Ni-doped CuO nanocomposite, the obtained diffraction peaks are unequivocally matched with JCPDS card no. 48-1548 except for peak at 30.53 ^{O} reveals that the obtained particles are CuO Nps with a monoclinic phase. The additional peaks matches with JCPDS card no. 89-5881, corresponding to NiO Nps, are also present in this sample. The average particle size is around 37 nm.

3.2 UV-Vis spectrometer

Semiconductor materials' UV-visible absorption spectra are deemed to be highly valuable instruments that depend on a multitude of factors, including surface morphology, doping, and the materials' interaction with the environment. The electronic states in the high energy region of the optical absorption spectrum are quite clarified by analyzing the spectral behavior of the absorption coefficient of any semiconducting material; atomic vibrations are represented in the lower energy region of the spectrum. It emerged that the optical spectra of these materials also exhibit three primary zones. They are the following: [29] absorption edge region, [30] strong absorption region and [31] weak absorption region. In the UV-visible spectrum, a weak absorption zone is associated with impurities, while a strong absorption region is caused by pure material and is related to the optical band gap energy of the substance. The structure disorder that results from doping or substitution in the material causes the absorption edge region to appear. The UV-visible spectra of NiO and CuO nanoparticles are displayed in figure 2(a,

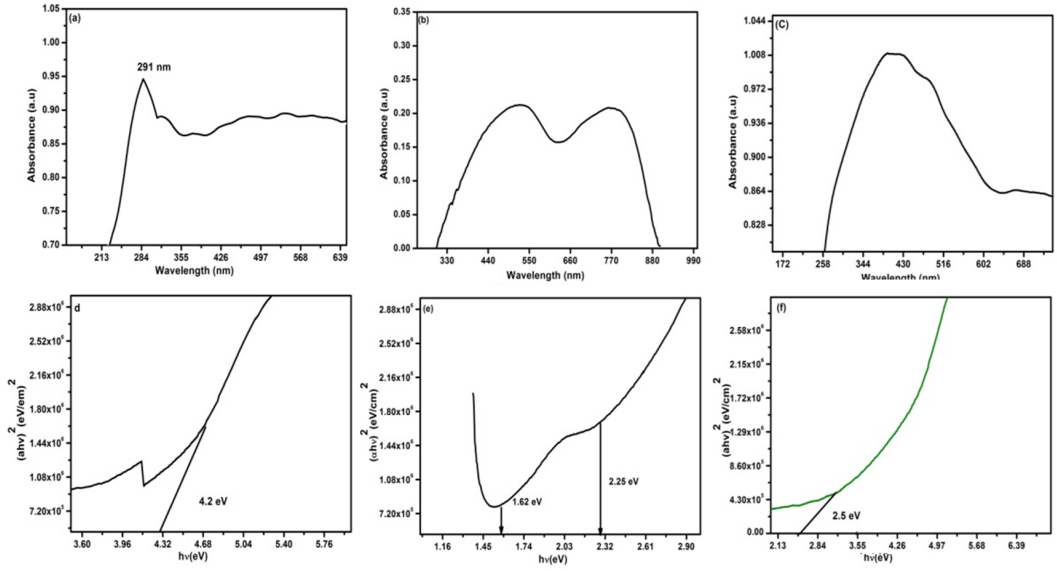

Figure 2. (a-f). Show the UV absorbance spectra graph and Tauc's plot.

c). NiO was discovered to have strong absorption at 291 nm. The CuO Nps were corroborated by two absorption peaks. Their broad range of wavelengths, ranging from (450 to 550 nm) to (740 to 801 nm), is explained by the d-d transition band. UV-visible spectra of CuO nanoparticles replaced with Ni are displayed in figure 2(e). It was found that absorption bands were moved to a lower wavelength, between 393 to 431 nm, when Ni was substituted. This happens because of an assortment of causes, including oxygen stoichiometry, size, and the quantum confinement effect; it may additionally happen because of Ni clustering and an increase in the surface area to volume ratio [32].

The band gap of a material is believed to be an essential indicator of its ability to be excited by incident photons and thus dictates its potential uses in optoelectronics [33]. Tauc's formula was used to determine the samples' E_g values.

$$(\alpha h\nu) = A(h\nu - E_g)^n \quad (1)$$

In equation 1, α = molar absorptivity, A = measured absorbance, h = Plank's constant, ν = frequency of light, n is constant and related to mode of transition and E_g = band gap energy. Value of n is 1/2 for direct band gap and 2 for indirect band gap. As illustrated in Fig. 2, (b, d, e, f), plotted between "$h\nu$" and $(\alpha h\nu)^{1/n}$, band gap energy was computed by extrapolating the graph's straight section. NiO was found to have very high band gap energy of 4.2 eV [32]. The band gap values were 2.25 eV and 1.62 [33] eV, confirming the validity of CuO Nps synthesis. Compared to pure CuO Nps, it became apparent that the bandgap energy of Ni-substituted CuO increased to 2.5 eV [34]. As an outcome, nickel oxide's impact caused the optical energy band gap to increase in value. [35]. this can also be explained by the fact that Ni doping reduced the particle size. The well-known semiconductor quantum confinement effect is caused by the reduction in particle size [36–39].

3.3 FTIR studies

An analysis method for establishing a molecule's vibrational frequency band and investigating the surface characteristics of CuO nanoparticles is Fourier transform infrared spectroscopy [40, 41]. Figure 3 shows the Fourier transform infrared spectra (FTIR) analysis of pure NiO, pure CuO, and Ni - doped CuO nanocomposites in the 400–4000 cm^{-1} range. The peak at 435.06 cm^{-1} is attributed to NiO Nps, the weak band at 1632.98 cm^{-1} is ascribed to the bending mode of H_2O molecules, the band at 1101.38 cm^{-1} is due to C – H bending vibrations for NiO Nps and the band appears at 3445.18 cm^{-1} is assigned to water molecules. The presence of water molecules is owing to adsorption on the NiO surface when NiO Nps are exposed to the atmosphere. In FTIR analysis of pure CuO Nps, the narrow bands at 462.82 and 581.82 $cm^{-1}$are powerful Cu - O stretching vibrations that confirm the formation of highly pure CuO Nps [42]. The band at 1107.28 is assigned to C - O stretching of alcoholic and phenol compounds [43] , and the peak at 1469 cm^{-1} denotes the O – H bending [44]. In FTIR analysis of Ni - doped CuO nanocomposite, all observed bands are found to be shifted towards a higher wave-number side than CuO Nps. This shift can be due to Ni doping ions in the CuO host lattice [45]. A significant finding in the FTIR study of the Ni-doped CuO nanocomposite is the slight shift of all typical peaks into higher wave numbers. This shift can be explained by the variation in bond length between Cu, Ni, and O ions that results from the replacement of Cu ions with Ni ions. CuO Nps are verified by the bands at 480.26 and 581.82 cm^{-1}, while the band at 1124.28 cm^{-1} is caused by the C - O stretching of phenol and an alcohol molecule [46, 47].

3.4 Morphological and elemental studies

The morphology was studied using by FESEM, and the compositional analysis was done by EDAX spectrum which were illustrated in figure 4(a, b, c, and d) and 5(a, b, and c). It depicts the presence of cubic-shaped NiO Nps and

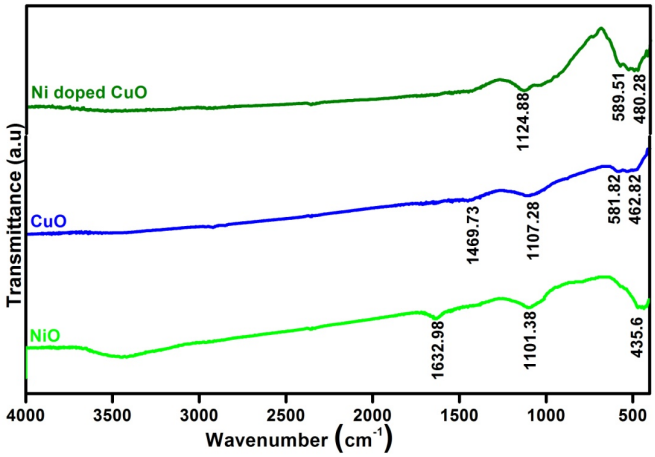

Figure 3. FTIR spectra of pure NiO Nps, pure CuO Nps, and Ni doped CuO nanocomposite.

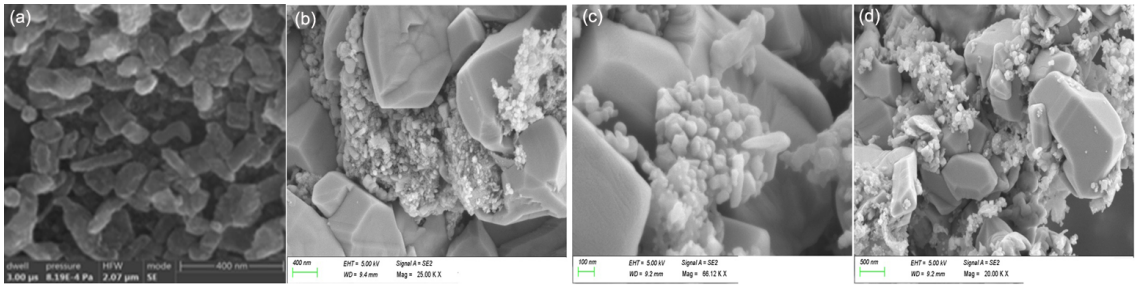

Figure 4. FESEM of a) pure Nio, b) pure CuO, and (c and d) Ni doped CuO nanocomposite.

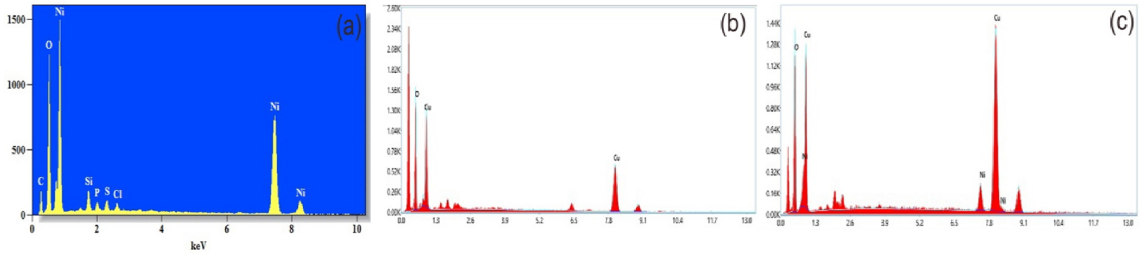

Figure 5. EDAX of e) pure NiO, f) pure CuO, and g) Ni doped CuO nanocomposite.

tiny rods [48]. The pure copper oxide Nps show particle aggregation with leaf - like formations, and when it is doped with Ni, it shows a mixture of structures, i.e., rod, prismatic, spherical, and hexagonal structures. The EDAX spectrum is used to determine the elemental presence of prepared Nps, confirming the presence of pure NiO and CuO Nps. It shows the presence of 59.27 % of Ni and 28.13 per cent of O and 66.79 % of Cu, and 33.21 % of O. When Ni is added to CuO Nps; it shows the presence of 71.13 % of copper, 26.50 % of oxygen and 2.37 % of Nickel. Due to the plant extract, some traces of Phosphor and Sulphur are seen. The carbon peaks in the spectrum is due to copper support grid (coated with carbon) used in the EDAX analysis.

3.5 The electrochemical analysis

The Cyclic Voltammetry examined the electrochemical capacitive behaviour for NiO, CuO, and Ni-doped CuO nanocomposites. The prepared Nps were evaluated under conventional functioning events at various scan rates in the potential window of 0.1–0.6 V using a 2 M KOH electrolyte. The specific capacitance Csp (F / g) was calculated using the Eq. 2.

$$C_{sp} = \frac{I\Delta t}{2mv\Delta v} \tag{2}$$

The CV curves for an as-prepared CuO, NiO, and Ni-doped CuO nanocomposites electrode in 2M KOH at scan speeds ranging from 10 to 100, mV/s are illustrated in figure 6. The scan rate is directly correlated with the area under the CV. According to the graph, the NiO, CuO, and Ni-doped CuO nanocomposite have optimum specific capacitances of approximately 260.89 F/g, 175.89 F/g, and 314.64 F/g at a rate of 10 mV/s, while its lowest specific capacitances are about 63.28 F/g, 49.02 F/g, and 150.268 F/g at a rate of 100 mV/s. Significant capacitance values are shown for the NiO, CuO, and Ni-doped CuO nanocomposite in figure 7 at a scan rate of 10 mV/s. Notably, compared to CuO Nps, the specific capacitance of the Ni - doped CuO nanocomposite is greater. The physical and chemical characteristics of CuO NPs may have changed as a result of the dopant Ni^{2+} addition. When the rate of scanning increases, the

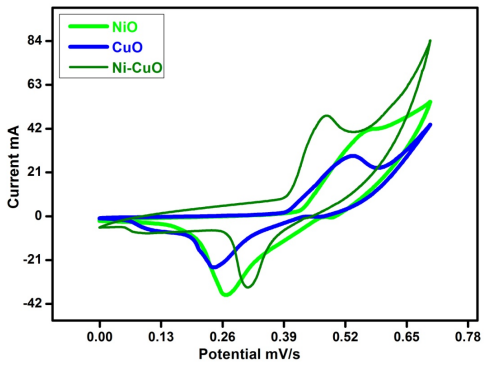

Figure 6. CV graph of pure NiO NPs, pure CuO NPs, Ni doped CuO nanocomposite.

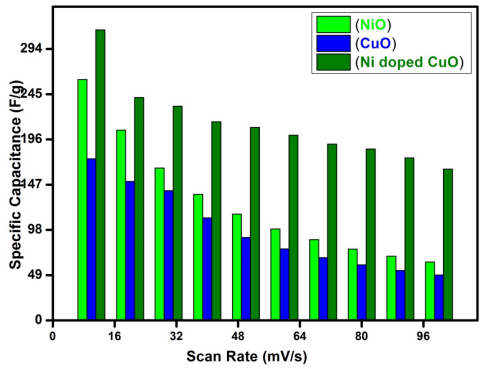

Figure 7. Scan rate versus specific capacitance.

anodic and cathodic current peaks always rise gradually. It implies a diffusion-limited redox chemical reaction as the mechanism of charge storage. The redox process may be quasi-irreversible since the anodizing peak potential shifts in a positive direction due to the kinetic constraint. [54] We further examined the electrochemical performances of CuO, NiO, and Ni-doped CuO nanocomposites at constant current densities using a charged-discharge analysis. The charge - discharge analysis curves (in Figs. 8a, b, c) illustrate the variation in current densities between 1 and 5 A/g within the potential range of 0.1 and 0.5 V. For CuO, NiO, and Ni - doped CuO nanocomposites, the specific capacitance values range from 122 to 65 F/g, 229 to 79.87 F/g, and 165 to 100 F/g (Table 1). This indicates that the fabrication of Ni - doped CuO nanocomposites maintains their outstanding stability and increases their high specific capacitance. These experimental findings substantiate the Ni - doped CuO nanocomposites' pseudocapacitance behavior and imply that they might provide suitable substances for electrodes for Li - ion batteries and supercapacitors. Additionally, our generated samples and the capacitance of previously reported CuO materials were evaluated, as shown in Table 2.

3.6 Antibacterial studies

The antibacterial tests were carried out based on reports from Azam et al., [55] and Paul Debashri et al., [56] on gram-positive bacteria such as Staphylococcus aureus and Bacillus stereus and gram-negative bacteria such as Escherichia coli and Pseudomonas aeruginosa using NiO Nps (Fig. 9), CuO Nps, and Ni doped CuO nanocomposite (Fig. 10). The bactericidal mechanism completed in 3 steps: (i) the production of ROS, (ii) rupture of microbial cell wall (iii) discharge of ions [57]. Researchers looked at data on antibacterial activity. They found that nanocomposites make reactive oxygen species (ROS) that kill bacteria. The production of reactive oxygen species (ROS) is facilitated by various factors such as specific surface area, oxygen vacancies contained by nanocomposites, diffusion potential of reactant molecules, and discharge of Ni^{2+}, Cu^{2+}, and Cu^{1+} ions. The presence of hydrogen peroxide (H_2O_2), hydroxyl radical (OH), and superoxide (O^{2-}) in ROS can break down cellular and DNA coverings, leading to significant damage to pathogen cells. This enhances the antibacterial potential displayed by ni-doped copper oxide nanocomposites, and it can be concluded that comparatively more ROS production is required to effectively kill bacterial strains [58–63]. As demonstrated in Table 2, it was clear that Gram-negative

Table 1. Comparisons of specific capacitance of CuO NPs, and Ni doped CuO nanocomposites.

Nanocomposite material	Specific capacitance	Electrolyte	Reference
$Cu/Cu_2O/ZnO/CuO$	241 F/g (50 mV/s)	KOH	[49]
$(CuO\text{-}Cu_2O)$ Cu	178.68 F/g (0.01 mV/s)	1M KCl	[50]
CeO_2-CuO	396 F/g at a current density of 1 A/g	1M $LiClO_4$	[51]
Zno-cuo	260.7 F/g (100 mV/s)	1M H_2SO	[52]
Cu/CuO nanobuds	0.7 A/g 230 31	6M KOH	[53]
Cu/CuO nanoflowers	0.7 A/g 296	6M KOH	[53]
MnO_2-CuO	279.12 F/g	1M KOH	
Ni doped CuO nanocomposite	314.64 F/g (10 mV/s)	2 M KOH	Current work

Table 2. Antibacterial activities of pure CuO NPs, and Ni doped CuO nanocomposites.

	Inhibition zone in mm		
Bacteria	NiO	CuO	Ni doped CuO
E.coli	14.5	16	17
Staphylococcus aureus	13	15	16
Bacillus cereus	15	16	18
Pseudomonas aeruginosa	13	14	16.5

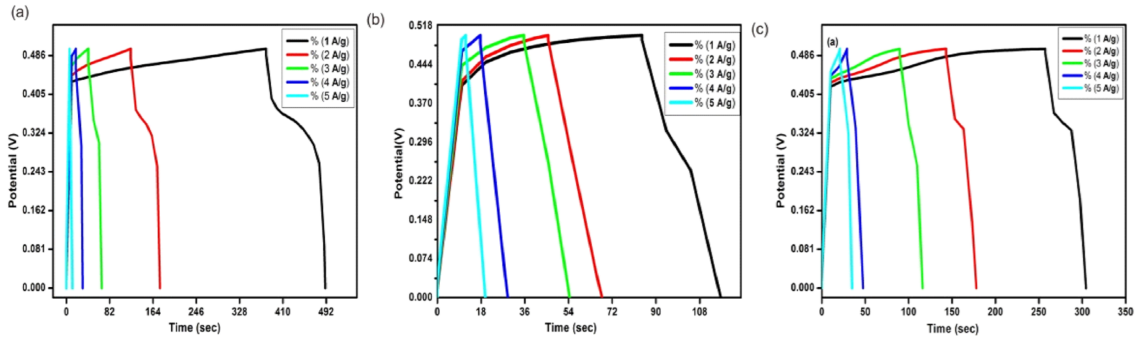

Figure 8. GCD curves of a) pure NiO NPs, b) pure CuO NPs, and c) Ni doped CuO nanocomposite.

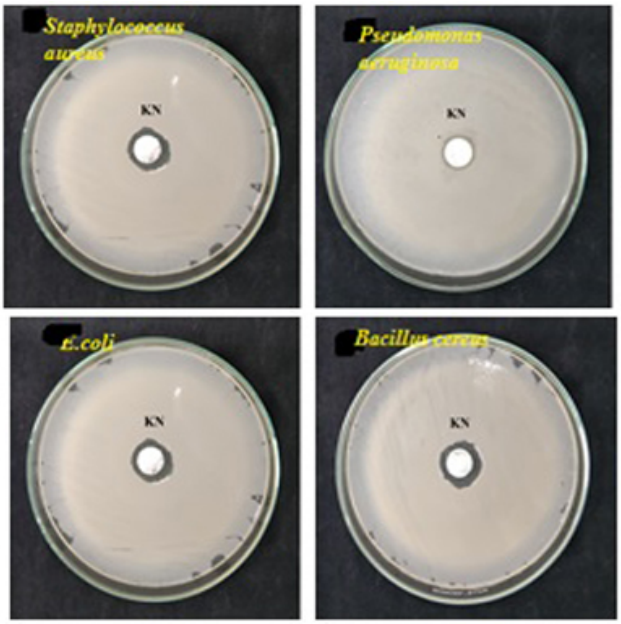

Figure 9. Antibacterial activity of pure NiO NPs.

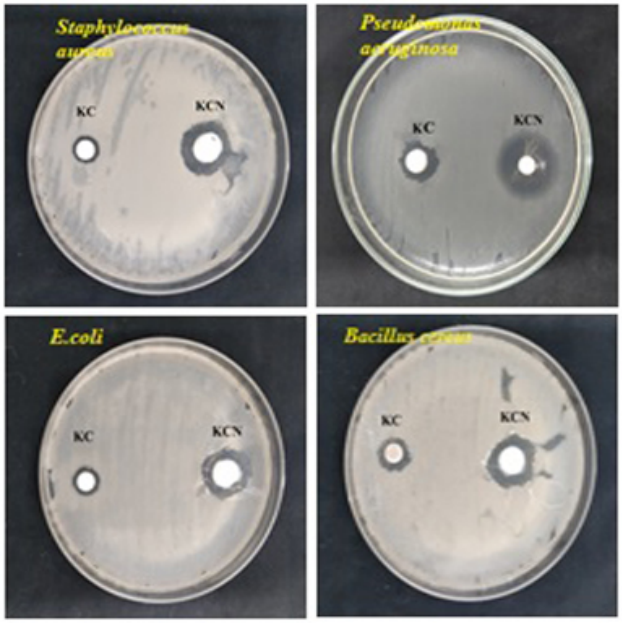

Figure 10. Antibacterial studies of pure CuO NPs, and Ni doped CuO nanocomposites.

bacteria were more susceptible to the antibacterial properties of Ni-doped CuO samples than gram-positive bacteria [64, 65]. Gram-positive bacteria have thicker peptidoglycan cell membranes, which make them more difficult to penetrate. The bacterial cell wall was rendered less resistant to nanoparticles by the outside bacterial membrane. Because metal oxide nanoparticles have a remarkably high surface-to-volume ratio, they interact with bacterial cell membranes through their surfaces in microorganisms. Due to the bacterium's eventual demise, this causes the nanoparticles to aggregate on the cell surface [66, 67]. Furthermore, the surface functionalization of NPs affects a path that aims to highlight and/or list unique characteristics that are helpful in applications related to biomedicine [68]. Additionally, the antibacterial effects of the Ni-doped CuO nanocomposite exceed those of pure CuO Nps. The multi-drug resistance of common bacteria in living things is caused by these antibacterial substances, which are also used for biological purposes as antibacterial agents in the food processing and production sectors. Ni-doped CuO nanocomposites are an exciting replacement for these substances [69].

4. Conclusion

This work illustrated the environmentally benign, straightforward, and effective biosynthesis of NiO Nps, CuO Nps, and Ni-doped CuO nanocomposite utilizing *Centraturam punctuatum* leaf extract. Cyclic voltammetry verified the pseudo-capacitance in nature by detecting a high specific capacitance in the nickel-doped copper oxide nanocomposite. Due to its excellent electrochemical stability, it can be used as a potential electrode for capacitor applications. Compared to copper oxide Nps, the nickel-doped copper oxide nanocomposite exhibits significantly stronger antibacterial activity. In light of these findings, we anticipate that these materials might offer researchers innovative ideas and novel applications, primarily in the biomedical and pharmaceutical sectors and in the control of antibiotic use.

Aknowledgements
Mrs. S. Subha (Reg,No: 19122232132023) is thankful to authorities of V. O. Chidambaram College, Thoothukudi and Manonmaniam Sundaranar University, Abishekapatti, Tirunelveli, Tamilnadu, India for providing necessary research facilities.

Authors contributions
Authors have contributed equally in preparing and writing the manuscript.

Availability of data and materials
The data that support the findings of this study are available from the corresponding author upon reasonable request.

Conflict of interests
The authors declare that they have no known competing financial interests or personal relationships that could have appeared to influence the work reported in this paper.

References

[1] M. Ghane, B. Sadeghi, A. R. Jafari, and A. R. Paknejhad. Synthesis and characterization of a bi-oxide nanoparticle zno/cuo by thermal decomposition of oxalate precursor method. *Int. J. Nano Dim*, 1: 33–40, 2010.
DOI: https://doi.org/10.7508/IJND.2010.0X.003.

[2] K. Vishveshvar, M. Aravind Krishnan, K. Haribabu, and S. Vishnuprasad. Green synthesis of copper oxide nanoparticles using ixiro coccinea plant leaves and its characterization. *BioNanoSci*, 8:554–558, 2018.
DOI: https://doi.org/10.1007/s12668-018-0508-5.

[3] W. J. Stark, P. R. Stoessel, and W. Wohlleben A. Hafner. Industrial applications of nanoparticles. *Chem. Soc. Rev*, 44:5793–5805, 2015.
DOI: https://doi.org/10.1039/C4CS00362D.

[4] L. Arun, C. Karthikeyan, D. Philip, D. Dhayanithi, N. V. Giridharan, and C. Unni. Influence of transition metal ion ni 2+ on optical,

electrical, magnetic and antibacterial properties of phyto-synthesized cuo nanostructure. *Opt. Quantum Electron*, 50(1-19), 2018. DOI: https://doi.org/10.1007/s11082-018-1684-9.

[5] M. Iqbal, A. Ali, K. S. Ahmad, F. M. Rana, J. Khan, and K. H. Thebo. Synthesis and characterization of transition metals doped cuo nanostructure and their application in hybrid bulk heterojunction solar cells. *SN Appl. Sci*, 1(1-8), 2019. DOI: https://doi.org/10.1007/s42452-019-0663-5.

[6] P. Vomacka, V. Stengl, J. Henych, and M. Kormunda. Shape-controlled synthesis of sn-doped cuo nanoparticles for catalytic degradation of rhodamine b. *J. Colloid Interface Sci*, 481:28–38, 2016. DOI: https://doi.org/10.1016/j.jcis.2016.07.026.

[7] K. Balakrishnan, G. Thangavel, and N. Murugesan. Structural, morphological, optical and electrochemical aspects of novel synthesized nickel oxide and cobalt doped nickel oxide nanoparticles–an alternate electrode material for energy storage devices. *Int. J. Nano Dim*, 14:191–202, 2023. DOI: https://doi.org/10.22034/IJND.2023.1981971.2209.

[8] S. P. Jahromi, N. M. Huang, M. R. Muhamad, and H. N. Lim. Green gelatine-assisted sol–gel synthesis of ultrasmall nickel oxide nanoparticles. *Ceram. Int*, 39:3909–3914, 2013. DOI: https://doi.org/10.1016/j.ceramint.2012.10.237.

[9] T. N. J. I. Edison, R. Atchudan, and Y. R. Lee. Binder-free electrosynthesis of highly ordered nickel oxide nanoparticles and its electrochemical performance. *Electrochim. Acta*, 283:1609–1617, 2018. DOI: https://doi.org/10.1016/j.electacta.2018.07.101.

[10] M. A. Nasseri, F. Kamali, and B. Zakerinasab. Catalytic activity of reusable nickel oxide nanoparticles in the synthesis of spirooxindoles. *RSC Adv*, 5:26517–26520, 2015. DOI: https://doi.org/10.1039/C5RA02825F.

[11] K. Kannan, D. Radhika, S. Vijayalakshmi, K. K. A. Sadasivuni, A. Ojiaku, and U. Verma. Facile fabrication of cuo nanoparticles via microwave-assisted method: photocatalytic, antimicrobial and anticancer enhancing performance. *Int. J. Environ. Anal. Chem*, 102: 1095–1108, 2022. DOI: https://doi.org/10.1080/03067319.2020.1733543.

[12] G. A. Rather, A. Nanda, M. A. Pandit, S. Yahya, H. Barabadi, and M. Saravanan. Biosynthesis of zinc oxide nanoparticles using bergenia ciliate aqueous extract and evaluation of their photocatalytic and antioxidant potential. *Inorg. Chem. Commun*, 134:109020, 2021. DOI: https://doi.org/10.1016/j.inoche.2021.109020.

[13] A. R. G. Ghomi, M. Mohammadi-Khanaposhti, H. Vahidi, F. Kobarfard, M. A. S. Reza, and H. Barabadi. Fungus-mediated extracellular biosynthesis and characterization of zirconium nanoparticles using standard penicillium species and their preliminary bactericidal potential: a novel biological approach to nanoparticle synthesis. *Iran. J. Pharm. Res*, 18:2101–2110, 2019. DOI: https://doi.org/10.22037/ijpr.2019.112382.13722.

[14] H. Vahidi, F. Kobarfard, A. Alizadeh, M. Saravanan, and H. Barabadi. Green nanotechnology-based tellurium nanoparticles: Exploration of their antioxidant, antibacterial, antifungal and cytotoxic potentials against cancerous and normal cells compared to potassium tellurite. *Inorg. Chem. Commun*, 124:108385, 2021. DOI: https://doi.org/10.1016/j.inoche.2020.108385.

[15] K. Rayapa Reddy. Green synthesis, morphological and optical studies of cuo nanoparticles. *J. Mol. Struct*, 1150:553–557, 2017. DOI: https://doi.org/10.1016/j.molstruc.2017.09.005.

[16] F. Ijaz, S. Shahid, S. A. Khan, W. Ahmad, and S. Zaman. Green synthesis of copper oxide nanoparticles using abutilon indicum leaf extract: Antimicrobial, antioxidant and photocatalytic dye degradation activities. *Trop. J. Pharm. Res*, 16:743–753, 2017. DOI: https://doi.org/10.4314/tjpr.v16i4.2.

[17] P. P. N. Vijay Kumar, U. Shameem, P. Kollu, R. L. Kalyani, and S. V. N. Pammi. Green synthesis of copper oxide nanoparticles using aloe vera leaf extract and its antibacterial activity against fish bacterial pathogens. *BioNanoSci*, 5:135–139, 2015. DOI: https://doi.org/10.1007/s12668-015-0171-z.

[18] V. V. T. Padil and M. Černík. Green synthesis of copper oxide nanoparticles using gum karaya as a biotemplate and their antibacterial application. *Int. J. Nanomed*, 8:889–898, 2013. DOI: https://doi.org/10.2147/IJN.S40599.

[19] N. K. Pawar and N. Arumugam. Leaf extract of centratherum punctatum exhibits antimicrobial, antioxidant and anti proliferative properties. *Asian J. Pharm. Clin. Res.*, 4:71–76, 2011.

[20] B. Chitra and P. Brindha. Studies on preliminary phytochemical screening of different extracts of centratherum punctatum cass. - a traditional wound healer. *Int. J. Pharm. Pharm. Sci*, 6:19–22, 2014.

[21] R. Sivasubramanian and P. Brindha. In-vitro cytotoxic, antioxidant and gc-ms studies on centratherum punctatum cass. *Int. J. Pharm. Pharm. Sci.*, 5:364–367, 2013.

[22] P. Satyal, V. Ho, U. Hie, T. Do, N. Thi I. La, B. Ngoc, N. C. Huy, D. Nang, and W. N. Setzer. The essential oil compositions of centratherum punctatum growing wild in vietnam. *Am. J. Essent. Oil Nat. Prod*, 6:15–18, 2018.

[23] K. S. Shankaran, S. A. Ganai, K. P. Arun, B. Brindha, and M. Vijalakshmi. In silico and in vitro evaluation of the anti-inflammatory potential of centratherum punctatum cass-a. *J. Biomol. Struct. Dyn*, 35:765–780, 2017. DOI: https://doi.org/10.1080/07391102.2016.1160840.

[24] B. Chitra and P. Brindha. Antimicrobial activity of ethanol and aqueous extracts of centratherum punctatum cass. *World J. Pharm. Pharm. Sci*, 4:1126–1131, 2015.

[25] J. C. Chukwujekwu, A. R. Ndhlala, C. A. De Kock, P. J. Smith, and J. Van Staden. Antiplasmodial, hiv-1 reverse transcriptase inhibitory and cytotoxicity properties of centratherum punctatum cass and its fractions. *S. Afr. J. Bot*, 90:17–19, 2014. DOI: https://doi.org/10.1016/j.sajb.2013.10.001.

[26] B. Chitra, P. Brindha, and A. B. Vijayakumar. Protease activity of floral extracts of centratherum punctatum cass.a wound healing herb. *World J. Pharm. Res*, 5:1079–1083, 2016. DOI: https://doi.org/10.1016/j.sajb.2013.10.001.

[27] S. T. Fardood, A. Ramazani, and S. Moradi. A novel green synthesis of nickel oxide nanoparticles using arabic gum. *Chemistry Journal of Moldova. General, Industrial and Ecological Chemistry*, 12:115–118, 2017. DOI: https://doi.org/10.19261/cjm.2017.383.

[28] S. Ghazal, A. Alireza, H. A. Hosseini, Z. Sabouri, F. Forouzanfar, M. Khatami, and M. Darroudo. Sol gel biosynthesis of nickel oxide nanoparticles using cydoniaoblonga extract and evaluation of their cytoxicity and photocatalytic activities. *J. Mol. Struct*, 1217:128378, 2020. DOI: https://doi.org/10.1016/j.molstruc.2020.128378.

[29] S. Yousaf, S. Zulfiqar, M. N. Shahi, M. F. Warsi, N. F. Al-Khalli, M. F. A. Aboud, and I. Shakir. uning the structural, optical and electrical properties of nio nanoparticles prepared by wet chemical route. *T Ceram. Int*, 46:3750–3758, 2020. DOI: https://doi.org/10.1016/j.ceramint.2019.10.097.

[30] Hassanien A. S.and Akl A. A. Effect of se addition on optical and electrical properties of chalcogenide cdsse thin films. *Superlattice Microstruct*, 89:153–169, 2016. DOI: https://doi.org/10.1016/j.spmi.2015.10.044.

[31] P. C. Udayabhanu, M. A. Nethravathi, D. Pavan Kumar, K. Suresh, H. Lingaraju, H. Rajanaika, and S. C. S. Nagabhushana. Tinospora cordifolia mediated facile green synthesis of cupric oxide nanoparticles and their photocatalytic, antioxidant and antibacterial properties. *Mater. Sci. Semicond. Process*, 33:81–88, 2015. DOI: https://doi.org/10.1016/j.mssp.2015.01.034.

[32] A. Pramothkumar, N. Senthilkumar, K.C. Mercy Gnana Malar, M. Meena, and I. V. Pothekar. A comparative analysis on the dye degradation efficiency of pure, co, ni and mn-doped cuo nanoparticles. *J. Mater. Sci.: Mater. Electron*, 30:19043–19059, 2019.
DOI: https://doi.org/10.1007/s10854-019-02262-4.

[33] M. N. Siddique, A. Ahmed, T. Ali, and P. Tripathi. Investigation of optical properties of nickel oxide nanostructures using photoluminescence and diffuse reflectance spectroscopy. *AIP Conf. Proc*, 1953: 030027, 2018.
DOI: https://doi.org/10.1063/1.5032362.

[34] Z. Sabouri, A. Rangrazi, M. S. Amiri, M. Khatami, and M. Darroudi. Green synthesis of nickel oxide nanoparticles using salvia hispanica l. (chia) seeds extract and studies of their photocatalytic activity and cytotoxicity effects. *Bioprocess Biosyst. Eng*, 44:2407–2415, 2021.
DOI: https://doi.org/10.1007/s00449-021-02613-8.

[35] M. W. Alam, M. Aamir, M. Farhan, M. Albuhulayqah, M. M. Ahmad, C. R. Ravikumar, V. G. Dileep Kumar, and H. C. Ananda Murthy. Green synthesis of ni-cu-zn based nanosized metal oxides for photocatalytic and sensor applications. *Crystals*, 11:1467, 2021.
DOI: https://doi.org/10.3390/cryst11121467.

[36] K. Lingarajua, H. Raja Naika, H. Nagabhushana, S. Devaraja K. Jayanna and, and G. Nagaraju. Biosynthesis of nickel oxide nanoparticles from euphorbia heterophylla (l.) and their biological application. *Arabian J. Chem*, 13:4712–4719, 2019.
DOI: https://doi.org/10.1016/j.arabjc.2019.11.003.

[37] J. Oh, H. Ryu, W. J. Lee, and J. S. Bae. Improved photostability of a cuo photoelectrode with ni-doped seed layer. *Ceram. Int.*, 44:89–95, 2018.
DOI: https://doi.org/10.1016/j.ceramint.2017.09.129.

[38] J. R. Aydın, A. Akkaya, and B. Sahin. Light-weight and flexible ni-doped cuo (ni:cuo) thin films grown using the cost-effective silar method for future technological requests. *Mater. Sci: Mater. Electron*, 33:23806–23820, 2022.
DOI: https://doi.org/10.1007/s10854-022-09139-z.

[39] L. M. Dwivedi, N. Shukla, K. Baranwaln, S. Gupta, S. Siidique, and V. Singh. Gum acacia modified ni doped cuo nanoparticles: An excellent antibacterial material. *J. Clust. Sci*, 32:209–219, 2021.
DOI: https://doi.org/10.1007/s10876-020-01779-7.

[40] M. A. Ansari and N. Jahan. A novel co precipitation route for the synthesis of pure and ni doped cuo nanoparticles effect of doping on structural,optical and electrical properties. *Int. J. Nanosci. Nanotechnol*, 19:65–76, 2023.
DOI: https://doi.org/10.22034/IJNN.2023.555186.2219.

[41] S. A. Amri, M. S. Ansari, S. Rafique, M. Aldhahri, S. Rahimuddin, A. Azam, and A. Memic. Ni doped cuo nanoparticles: structural and optical characterizations. *Curr. Nanosci*, 11:191–197, 2015.
DOI: https://doi.org/10.2174/1573413710666141024212856.

[42] S. Sukumar, A. Rudrasenan, and D. P. Nambiar. Green-synthesized rice-shaped copper oxide nanoparticles using caesalpinia bonducella seed extract and their applications. *ACS Omega*, 5:1040–1051, 2020.
DOI: https://doi.org/10.1021/acsomega.9b02857.

[43] V. U. Siddiqui, A. Ansari, R. Chauhan, and W. A. Siddiqi. Green synthesis of copper oxide (cuo) nanoparticles by punica granatum peel extract. *Mater. Today Proc.*, 36:751–755, 2021.
DOI: https://doi.org/10.1016/j.matpr.2020.05.504.

[44] K. Vishveshvar, M. V. Aravind Krishnan, K.Haribabu, and S. Vishnuprasad. Green synthesis of copper oxide nanoparticles using ixiro coccinea plant leaves and its characterization. *BioNanoSci*, 8:554–558, 2018.
DOI: https://doi.org/10.1007/s12668-018-0508-5.

[45] L. M. Dwivedi, N. Shukla, K. Baranwal, S. Gupta, S. Siddique, and V. Singh. Gum acacia modified ni doped cuo nanoparticles: An excellent antibacterial material. *J. Cluster Sci*, 32:209–219, 2021.
DOI: https://doi.org/10.1007/s10876-020-01779-7.

[46] A. R. Maheo, M. V. B. Scholastica, and A. P. T. Augustine. Biosynthesis and characterization of eupatorium adenophorum and chitosan mediated copper oxide nanoparticles and their antibacterial activity. *Results Surf. Interfaces*, 6:100048, 2022.
DOI: https://doi.org/10.1016/j.rsurfi.2022.100048.

[47] P. Geetha, K.Ponsindhuja, S. Sankaralingam, N. S. Sivasankara, and M. P. Sugapriya. Green synthesis of copper nanoparticles obtained from pedalium murex. l (yanai nerunjil) and their antimicrobial activity. *Int. J. Res. Advent. Technol*, 7:2321–9637, 2019.

[48] K. C. Suresh and A. Balamurugan. Evaluation of structural, optical, and morphological properties of nickel oxide nanoparticles for multi-functional applications. *Inorg. Nano-Metal Chem*, 51:296–301, 2020.
DOI: https://doi.org/10.1080/24701556.2020.1770793.

[49] X. Fuku, K. Kaviyarasu, N. Matinise, and M. Maaza. Punicalagin green functionalized cu/cu_2o/zno/cuo nanocomposite for potential electrochemical transducer and catalyst. *Nanoscale Res. Lett*, 11: 386, 2016.
DOI: https://doi.org/10.1186/s11671-016-1581-8.

[50] B. Uma, K. S. Anantharaju, B. S. Suredra, K. Gurusantha, S. S. More, S. Meena, B. Hemavathi, and H. C. A. Murthy. Influence of ag on the structural, electrochemical, antibacterial, and photocatalytic performance of the (cuo–cu_2o) cu nanocomposite. *ACS omega*, 8: 9947–9961, 2023.
DOI: https://doi.org/10.1021/acsomega.2c07124.

[51] G. Manibalan, G. Murugadoss, R. Thangamuthu, P. Ragupathy, R. Mohan Kumar, and R. Jayavel. Enhanced electrochemical supercapacitor and excellent amperometric sensor performance of heterostructure ceo_2-cuo nanocomposites via chemical route. *Appl. Surf. Sci*, 456:104–113, 2018.
DOI: https://doi.org/10.1016/j.apsusc.2018.06.071.

[52] V. Senthilkumar, Y. S. Kim, S. Chandrasekaran, B. Rajagopalan, E. J. Kim, and J. S. Chung. Comparative supercapacitance performance of cuo nanostructures for energy storage device applications. *RSC. Adv*, 5:20553–20545, 2015.
DOI: https://doi.org/10.1039/C5RA00035A.

[53] K. Mohamed Racik, A. Manikandan, M. Mahendiran, P. Prabakaran, J. Madhavan, and M. Victor Antony Raj. Fabrication of manganese oxide decorated copper oxide (mno_2/cuo) nanocomposite electrodes for energy storage supercapacitor devices. *Physica E*, 119:114033, 2020.
DOI: https://doi.org/10.1016/j.physe.2020.114033.

[54] L. Arun, C. Karthikeyan, D. Philip, M. Sasikumar, E. Elaiyappillai, J. P. Merlin, and C. Unni. Effect of ni^{2+}doping on chemocatalytic and supercapacitor performance of biosynthesized nanostructured cuo. *J. Mater. Sci.: Mater. Electron.*, 29:21180–21193, 2018.
DOI: https://doi.org/10.1007/s10854-018-0268-6.

[55] D. Paul and N. Sudarsan. Synthesis, characterization and a comparative antibacterial study of cuo, nio and cuo-nio mixed metal oxide. *Mater. Res. Express*, 6::055004, 2019.
DOI: https://doi.org/10.1088/2053-1591/ab003c.

[56] A. Azam, A. S. Ahmed, M. Oves, M. S. Khan, S. S. Habib, and A. Memic. Antimicrobial activity of metal oxide nanoparticles against gram-positive and gram-negative bacteria: a comparative study. *Int. J. Nanomed*, 7:6003–6009, 2012.
DOI: https://doi.org/10.2147/IJN.S35347.

[57] K. Kumar, R. Kumar, R. Jasrotia, S. Kalia, V. Arya, A. Kumar, R. Khargotra, T. Singh, and N. Thakur. n-vitro bactericidal and antioxidant efficacy of biosynthesized cuo/cu_2o-nio nanocomposites against the pathogenic bacteria and dpph free radical. *I Discov. Appl. Sci*, 6:87, 2024.
DOI: https://doi.org/10.1007/s42452-024-05679-7.

[58] M. Hassanpour, H. Safardoust, D. Ghanbari, and M. S. Niasari. Microwave synthesis of cuo/nio magnetic nanocomposites and its application in photo-degradation of methyl orange. *J. Mater. Sci.: Mater. Electron*, 27:2718–2727, 2016.
DOI: https://doi.org/10.1007/s10854-015-4082-0.

[59] F. Sedighi, M. Esmaeili Zare, A. Sobhani-Nasab, and M. Behpour. Synthesis . *J. Mater. Sci.: Mater. Electron*, 29:13737–13745, 2018. DOI: https://doi.org/10.1007/s10854-018-9504-3.

[60] T. K. Jana, S. K. Maji, A. Pal, R. P. Maiti, T. K . Dolai, and K. Chatterjee. Photocatalytic and antibacterial activity of cadmium sulphide/zinc oxide nanocomposite with varied morphology. *J. Colloid Interface Sci*, 480:9–16, 2016. DOI: https://doi.org/10.1016/j.jcis.2016.06.073.

[61] V. Hoseinpour and G. Nasser. Novel zno–mno_2–cu_2o triple nanocomposite: Facial synthesis, characterization, antibacterial activity and visible light photocatalytic performance for dyes degradation-a comparative study. *Mater. Res. Express*, 5:085012, 2018. DOI: https://doi.org/10.1088/2053-1591/aad2c6.

[62] K. Karthik, S. Dhanuskodi, C. Gobinath, S. Prabukumar, and S. Sivaramakrishnan. Multifunctional properties of microwave assisted cdo–nio–zno mixed metal oxide nanocomposite: enhanced photocatalytic and antibacterial activities. *J. Mater. Sci.: Mater. Electron*, 29:5459–5471, 2018. DOI: https://doi.org/10.1007/s10854-017-8513-y.

[63] K. Lefatshe, C. M. Muiva, and L. P. Kebaabetswe. Extraction of nanocellulose and in-situ casting of zno/cellulose nanocomposite with enhanced photocatalytic and antibacterial activity. *Carbohydr. Polym*, 15:301–308, 2017. DOI: https://doi.org/10.1016/j.carbpol.2017.02.020.

[64] D. Kumar, H. Shukla, and N. Sharma. Antibacterial and morphological studies of plant-mediated synthesized cuo nanoparticles using azadirachta indica (neem) leaf extract. *Int. J. Nano Dim*, 13:197–204, 2022. DOI: https://doi.org/10.22034/IJND.2022.686826.

[65] P. B. Nagore, A. J. Ghoti, A. P. Salve, and K. Mane. Green synthesis of luminescent copper oxide nanoparticles using ginger lily leaves extract. *J. Inorg. Organomet. Polym. Mater*, 30:4229, 2020. DOI: https://doi.org/10.1007/s10904-020-01614-6.

[66] J. S. Tawale, K. K. Dey, R. Pasricha, K. N. Sood, and A. K. Srivastava. Synthesis and characterization of zno tetrapods for optical and antibacterial applications. *Thin Solid Films*, 519:1244–1247, 2010. DOI: https://doi.org/10.1016/j.tsf.2010.08.077.

[67] A. Almontasser and A. Parveen. Probing the effect of ni, co and fe doping concentrations on the antibacterial behaviors of mgo nanoparticles. *Sci. Rep*, 12:7922, 2022. DOI: https://doi.org/10.1038/s41598-022-12081-z.

[68] S. Majeed, M. Saravanan, M. Danish, N. A. Zakariya, M. N. M. Ibrahim, E. H. Rizvi, S. N. Andrabi, H. Barabadi, Y. K. Mohanta, and E. Mostafavi. Bioengineering of green-synthesized tat peptide-functionalized silver nanoparticles for apoptotic cell-death mediated therapy of breast adenocarcinoma. *Talanta*, 253:124026, 2023. DOI: https://doi.org/10.1016/j.talanta.2022.124026.

[69] P. S. M. Kumar, H. H. Kyaw, M. T. Z. Myint, L. Al-Haj, A. H. Al-Muhtaseb, M. Al-Abri, V. Thanigaivel, and V. K. Ponnusamy. Green route synthesis of nanoporous copper oxide for efficient supercapacitor and capacitive deionization performances. *Int. J. Energy Res.*, 44: 10682–10694, 2020. DOI: https://doi.org/10.1002/er.5712.